

Precisely positioned generation of CsPbBr_3 nano-light sources in a Cs_4PbBr_6 film by electron beam irradiation

*Tomoyasu Fujimaru¹, Kanta Hirai², Masato Inamata¹, Hiromu Tanaka¹, Midori Ikeuchi³,
Hidehiro Yamashita³, Mitsutaka Haruta⁴, Takehiko Tamaoka⁵, Naohiko Kawasaki⁵,
and Hikaru Saito ^{*3}*

¹ Interdisciplinary Graduate School of Engineering Sciences, Kyushu University, 6-1 Kasugakoen, Kasuga, Fukuoka 816-8580, Japan

² Department of Interdisciplinary Engineering, School of Engineering, Kyushu University, 6-1 Kasugakoen, Kasuga, Fukuoka 816-8580, Japan

³ Institute for Materials Chemistry and Engineering, Kyushu University, 6-1 Kasugakoen, Kasuga, Fukuoka 816-8580, Japan

⁴ Institute for Chemical Research, Kyoto University, Uji, Kyoto 611-0011, Japan

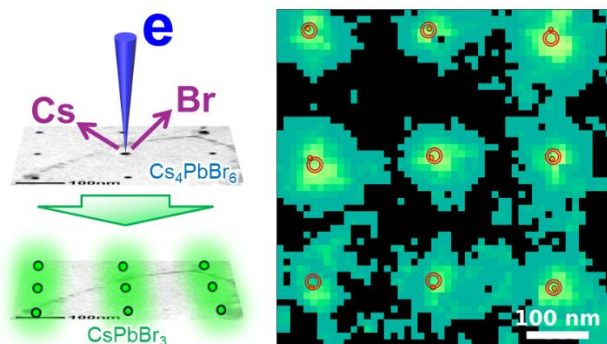
⁵ Morphological Research Laboratory, Toray Research Center Inc., Otsu, Shiga 520-8567, Japan

^{*}corresponding authors

ABSTRACT

Integration of high-quality photon emitters at specific locations within nanophotonic structures or optoelectronic devices is a key to innovating on-chip optical control and quantum technologies. Halide perovskite nanoparticles have great potential as single photon emitters with high quantum efficiency. To achieve their full potential, they must be embedded in a host material that ensures chemical stability and passivates surface defects. A previous experiment on a CsPbBr_3 – Cs_4PbBr_6 nanocomposite film suggested possibility that electron beam irradiation can be used to control positions of CsPbBr_3 nano-light sources in the Cs_4PbBr_6 host although the effects of electron beam irradiation are not fully understood. Here, we fabricate a Cs_4PbBr_6 – CsBr film, not containing the CsPbBr_3 phase, and provide direct evidence that CsPbBr_3 nanoparticles can be locally generated in the Cs_4PbBr_6 host by irradiation with a focused electron beam. We further demonstrate perovskite nano-light source arrays with submicron spacing using this method.

Table of Contents



KEYWORDS: nano-light source; halide perovskite; electron beam irradiation; cathodoluminescence; electron microscopy

Precise positioning of photon emitters at specific locations within nanophotonic structures is essential for advanced light control or quantum technologies, such as strong light-matter interactions or Fano interferences,¹⁻³ and spin-selective photon routing.⁴⁻⁶ Various top-down processes using electron beam lithography have been proposed for deterministic integration of quantum dots into on-chip optical circuits.⁷⁻¹⁰ Trapping excitons by locally introduced strain into transition metal dichalcogenides using nanostructures is a promising strategy to arrange quantum emitters and plasmonic resonators in proximity, achieving single-photon emitter arrays with a highly enhanced emission rate¹¹ and a control of spin angular momentum of single photon emitters.¹² Hexagonal boron nitride is also attracting great attention as a robust and versatile host for single photon emitters which can be introduced at precise locations by nanoindentation,¹³ irradiation with ion beams,¹⁴ electron beams,¹⁵ or lasers.¹⁶

However, such precise positioning of halide perovskite particles has not yet been reported, despite their excellent potential for highly efficient light-emitting diodes (LEDs),^{17,18} lasers,^{19,20} and single photon emitters functioning even at room temperature.^{21,22} To achieve this, we must find a nanoscale process to directly generate halide perovskite nanoparticles in a host material that ensures their chemical stability and passivates surface defects causing performance degradation.¹⁷ Tips to establish such a nanoscale process is seen in a previous experiment on a CsPbBr_3 – Cs_4PbBr_6 nanocomposite film, where electron beam irradiation increased green light emission from CsPbBr_3 nanoparticles in the film.²³ If this is due to the generation of CsPbBr_3 nanoparticles in the Cs_4PbBr_6 grains, electron beam irradiation can be used to control the positions of CsPbBr_3 nano-light sources. Cs_4PbBr_6 having a relatively wide bandgap of ~ 3.9 eV, is an excellent host material for confining charge carriers within embedded CsPbBr_3 nanoparticles having a narrower bandgap of ~ 2.3 eV.²⁴ In fact, photoluminescence yields of over 90% were measured from CsPbBr_3 nanoparticles

embedded in the Cs_4PbBr_6 host.²⁵ Furthermore, electroluminescence of CsPbBr_3 – Cs_4PbBr_6 nanocomposites demonstrated in previous studies^{26,27} also provides motivation to position-controlled CsPbBr_3 nano-light source generation in the Cs_4PbBr_6 host.

Here, we fabricate a film mainly composed of Cs_4PbBr_6 grains, excluding the CsPbBr_3 phase, and verify if CsPbBr_3 nanoparticles can be generated by irradiating Cs_4PbBr_6 with a focused electron beam. The changes in element ratios of the film caused by electron beam irradiation are revealed by energy-dispersive X-ray spectroscopy (EDS), the resulting nanoparticles are identified by electron energy-loss spectroscopy (EELS), and the light emission of the generated nanoparticles are characterized by cathodoluminescence (CL) spectroscopy.

RESULTS AND DISCUSSION

Characterization of fabricated films

In the previous experiment, green nano-light sources were formed by electron beam irradiation of CsPbBr_3 – Cs_4PbBr_6 nanocomposite film.²³ One possible interpretation was that new CsPbBr_3 nanoparticles were generated in the Cs_4PbBr_6 grains. However, that experiment also provided another interpretation that the light emission efficiency of the initially existing CsPbBr_3 nanoparticles was improved by some effects of electron beam irradiation. To verify the former possibility, we must prepare sufficiently large Cs_4PbBr_6 grains not containing CsPbBr_3 nanoparticles inside them. In this study, we fabricated two types of halide films by thermal evaporation. One is composed of well-separated Cs_4PbBr_6 and CsPbBr_3 grains obtained by annealing the CsPbBr_3 – Cs_4PbBr_6 nanocomposite film^{23,28} in vacuum at 250 °C for 30 min. The other is composed of Cs_4PbBr_6 and CsBr grains and free from the CsPbBr_3 phase. The details of film fabrication are provided in Method section. CL and EELS spectra obtained from Cs_4PbBr_6

and CsPbBr_3 grains in the former film were used as references when analyzing the changes of the latter film due to electron beam irradiation. The following scanning transmission electron microscopy (STEM)-based analysis was performed at a relatively low dose rate ($0.4 \text{ e/nm}^2/\text{ns}$ or less) and total dose ($2 \times 10^7 \text{ e/nm}^2$ or less), and no light source generation was recognized during this analysis.

Figure 1a shows a bright-field (BF) STEM image of the CsPbBr_3 – Cs_4PbBr_6 film. The white areas are pores without the CsPbBr_3 – Cs_4PbBr_6 layer. Such pores were not observed in the film without the post-annealing^{23,28} and were therefore formed during the annealing. Figure 1b shows a CL map obtained from the same field of view using a band-pass filter with the wavelength range of 500–550 nm, revealing that this film contains grains of several hundred nanometers that emit light in this wavelength range. The CL spectrum obtained from one of these bright grains

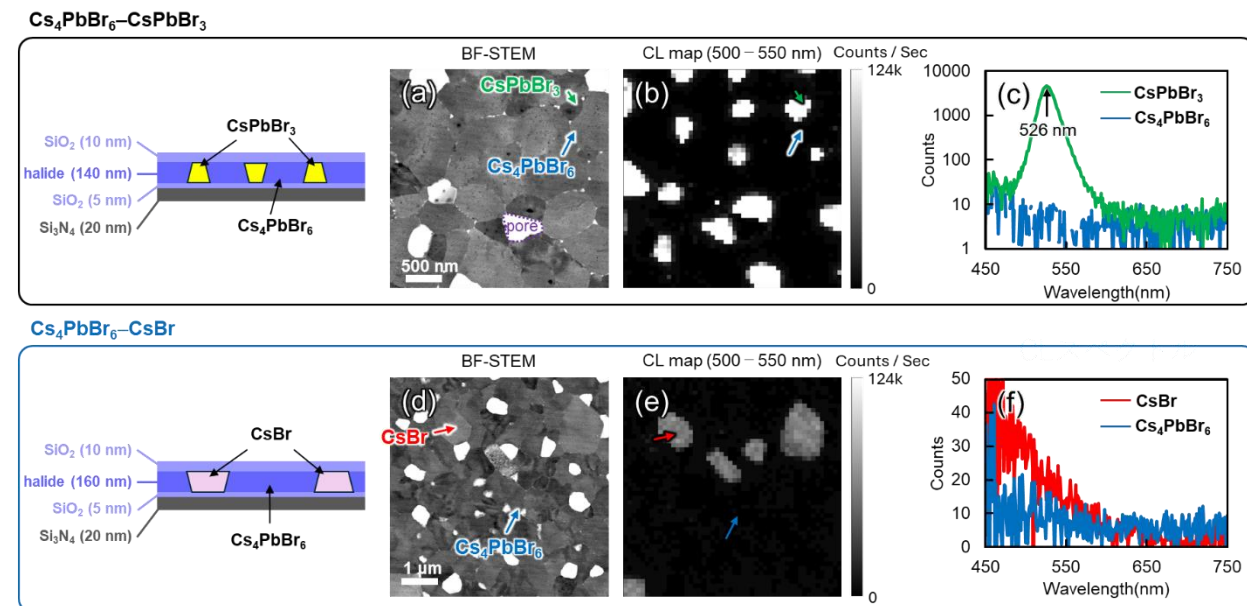


Figure 1 Structural analysis of the fabricated CsPbBr_3 – Cs_4PbBr_6 and Cs_4PbBr_6 – CsBr films by CL spectroscopy. (a) BF-STEM image, (b) CL map, and (c) CL spectra of the CsPbBr_3 – Cs_4PbBr_6 film. (d) BF-STEM image, (e) CL map, and (f) CL spectra of the Cs_4PbBr_6 – CsBr film. The CL maps were obtained with wavelength filtering from 500 to 550 nm. The CL spectra were obtained while irradiating the arrowed positions. Schematic structures of the CsPbBr_3 – Cs_4PbBr_6 and Cs_4PbBr_6 – CsBr films are shown in insets on the left of (a) and (d), respectively. All the measurements here were performed at a beam energy of 300 keV and a probe current of 200 pA.

(green arrow in Figs. 1a and b) has a peak wavelength of 526 nm (Fig. 1c), which is close to that of previously measured from micrometer-scale CsPbBr_3 particles.²⁹ On the other hand, no significant spectral features were observed in the visible range from the surroundings, which is consistent with the film being composed primarily of nonradiative Cs_4PbBr_6 grains.³⁰ In the film obtained without post-annealing, the CsPbBr_3 nanoparticles were dispersed evenly throughout the film, and CL maps showed a uniform intensity distribution at the nanoscale.²³ The post-annealing introduced in this study resulted in a structure separated into CsPbBr_3 and Cs_4PbBr_6 grains with sizes from several hundred nanometers to micrometers, allowing estimation of the phase volume ratio of CsPbBr_3 to be 23% from the bright area ratio in the CL map (Fig. 1b).

From the estimated CsPbBr_3 volume ratio, the amount of CsBr powder required to modify the element ratios of the evaporation source (CsPbBr_3 – Cs_4PbBr_6 nanocomposite powder) to $\text{Cs}:\text{Pb}:\text{Br} = 4:1:6$ was calculated, and the second film (Cs_4PbBr_6 – CsBr) was fabricated using the mixed evaporation source composed of CsPbBr_3 – Cs_4PbBr_6 nanocomposite powder and CsBr powder. Figures 1d and e show a BF-STEM image and a wavelength-filtered CL map of this modified film, respectively. The CL maps show several submicron- to micrometer-sized grains that are brighter than the surroundings (e.g. red arrow in Fig. 1d), but are much darker than CsPbBr_3 grains (Fig. 1b). The CL spectrum obtained from one of these slightly bright grains shows a broad peak in the shorter wavelength side (Fig. 1f), which is clearly different from that of CsPbBr_3 grains (Fig. 1c). To identify the chemicals consisting of this modified film, we analyzed it using EELS and EDS. In the annular dark-field (ADF)-STEM image, the above “slightly bright grains” appear in slightly darker intensity than the surroundings (e.g. area B in Fig. 2a). An EELS spectrum obtained from the surroundings (area A) shows peaks at 4 eV and 5.5 eV (Fig. 2b), which are consistent with those detected from Cs_4PbBr_6 particles.^{28,31} On the other hand, the slightly

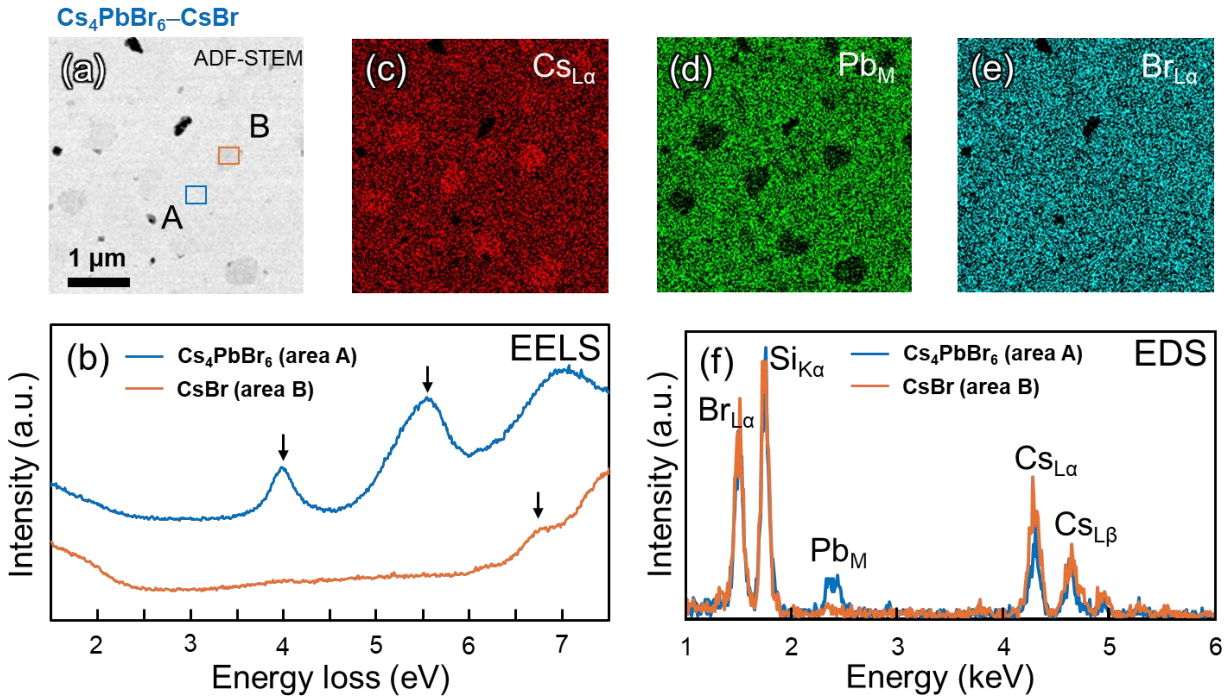


Figure 2 Structural analysis of the Cs_4PbBr_6 – CsBr film by EELS and EDS. (a) ADF-STEM image of the film. The blue (A) and orange (B) rectangles indicate extraction areas for the following EELS and EDS spectra. (b) EELS spectra obtained from a Cs_4PbBr_6 grain (area A) and a CsBr grain (area B). (c–e) Elemental maps using X-ray intensities at Cs_{La} , Pb_{M} , and Br_{La} lines, respectively. (e) EDS spectra obtained from a Cs_4PbBr_6 grain (area A) and a CsBr grain (area B). All the measurements here were performed at a beam energy of 80 keV. The probe current was 18 pA for EELS and 50 pA for EDS.

bright grain (area B) does not show any characteristic peaks below 6 eV, and the presence of a shoulder at 6.7 eV is consistent with that detected from CsBr .³² Elemental mapping by EDS shows that Pb is not detected in the slightly bright grains but instead the Cs density is increased compared to the surrounding area (Figs. 2c–f). Accordingly, by adjusting the element ratios as described above, this modified film is mainly composed of Cs_4PbBr_6 and free from CsPbBr_3 although it contains CsBr as a second phase probably due to an estimation error of the element ratios of the evaporation source. This film not only makes it straightforward to analyze the changes by electron beam irradiation, but also has advantages in the applications of nano-light sources since it does not contain background light sources.

Generation of CsPbBr_3 nano-light sources in Cs_4PbBr_6 grains by electron beam irradiation

Cs_4PbBr_6 grains in the prepared Cs_4PbBr_6 – CsBr film were irradiated using a focused electron beam and the changes at the irradiation points were investigated by CL, EELS, and EDS. Intense irradiation to modify Cs_4PbBr_6 grains was performed at a beam energy of 300 keV under “high dose conditions” with a dose rate of more than $1.5 \text{ e}/\text{nm}^2/\text{ns}$ and a total dose of more than $7.5 \times 10^9 \text{ e}/\text{nm}^2$. STEM-based analysis was performed at a beam energy of 80 or 300 keV under “low dose conditions” with a dose rate of less than $0.4 \text{ e}/\text{nm}^2/\text{ns}$ and a total dose of less than $2 \times 10^7 \text{ e}/\text{nm}^2$.

Figures 3a shows the first CL map obtained from a Cs_4PbBr_6 grain region at a beam energy of 300 keV under a low dose condition with a beam current of 200 pA and a beam diameter of 2 nm, and no meaningful signal is detected in this region. After this mapping, the four points (green arrows) were irradiated using a stopped beam under a high dose condition with a beam current of

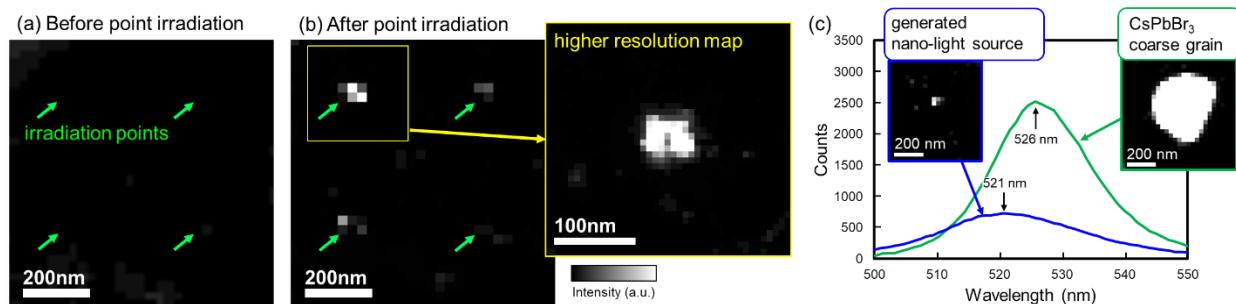


Figure 3 Point irradiation to Cs_4PbBr_6 grains in the Cs_4PbBr_6 – CsBr film with a focused electron beam and CL analysis of the generated nano-light sources. (a and b) CL maps (wavelength range: 500 to 550 nm) obtained before and after point irradiation. The green arrows indicate the four irradiation points. Each point was irradiated at a high dose rate of $1.5 \text{ e}/\text{nm}^2/\text{ns}$ (beam current: 3 nA, beam diameter: 4 nm) for 15 seconds corresponding to a total dose of $2 \times 10^{10} \text{ e}/\text{nm}^2$. A higher resolution CL map was obtained around one irradiation point (right inset of b). (c) CL spectrum acquired during point irradiation for 10 seconds (blue curve) at the high dose rate, which is compared with that obtained from an initially existing CsPbBr_3 coarse grain in the CsPbBr_3 – Cs_4PbBr_6 film (green curve). Wavelength-filtered CL maps of the generated nano-light source and the CsPbBr_3 coarse grain are shown in the insets. All the measurements here were performed at a beam energy of 300 keV and a probe current of 200 pA except for the CL spectrum acquired during the point irradiation (blue curve in c).

3 nA and a beam diameter of 4 nm for 15 seconds per point (s/point). The second CL map, shown in Fig. 3b, was then acquired from the same region under the same condition as the first map. Although the brightness and distribution vary point by point, bright spots appear at the four irradiation points while no significant changes are observed in the surrounding area. As discussed in the later subsection “Optimization of the irradiation time”, an irradiation time on the order of seconds is required to generate nano-light sources under the high dose conditions used here. Figure 3c shows the CL spectrum obtained by collecting light emission during point irradiation of another Cs_4PbBr_6 grain under a high dose condition for 10 seconds (blue curve). The inset CL map was obtained under a low dose condition after the 10 seconds of point irradiation, showing a nano-light source generated and grown during the 10 seconds. The CL peak wavelength was 521 nm, which is close to that of an initially existing CsPbBr_3 coarse grain in the CsPbBr_3 – Cs_4PbBr_6 film (green curve), but is slightly shifted to the shorter wavelength side due to the quantum size effect.^{33,34} A similar blue shift has been observed in the CL and photoluminescence of Cs_4PbBr_6 containing CsPbBr_3 nanoparticles.^{35,36}

We confirmed that the nano-light sources generated by electron beam irradiation are CsPbBr_3 nanoparticles by EELS measurements as discussed below. Figures 4a and b show a BF-STEM image and the corresponding wavelength-filtered CL map after irradiating nine points (green arrows) in Cs_4PbBr_6 grains under a high dose condition with a beam current of 8 nA and a beam diameter of 5 nm for 15 s/point. EELS mapping data was obtained from this area under a low dose condition, and two spectra were extracted near the central irradiation point (EELS1) and a surrounding area (EELS2) as shown in Fig. 4c. The spectra were analyzed using non-negative multiple linear least squares (MLLS) fitting assuming two components CsPbBr_3 and Cs_4PbBr_6 . Each reference spectrum was obtained from the CsPbBr_3 – Cs_4PbBr_6 film. This MLLS fitting was

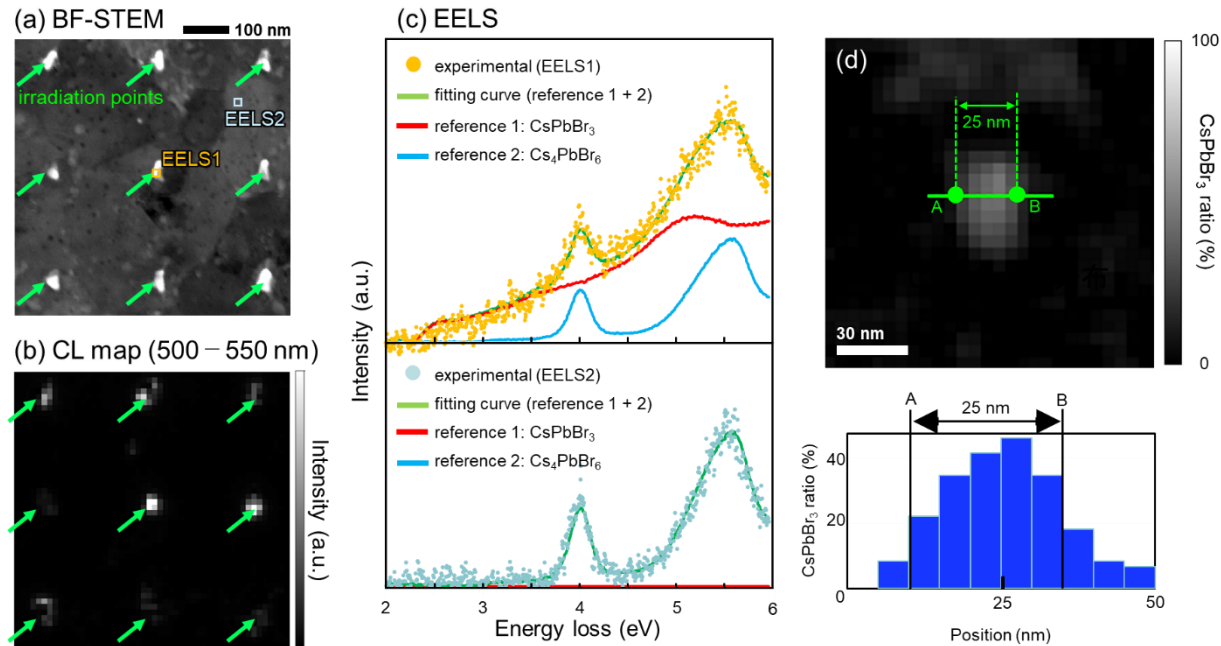


Figure 4 EELS analysis of the generated nano-light source in the Cs₄PbBr₆–CsBr film. (a and b) BF-STEM image and CL map (wavelength range: 500 to 550 nm) obtained after point irradiation. The green arrows indicate the nine irradiation points. Each point was irradiated at a beam energy of 300 keV and a high dose rate of 2.5 e/nm²/ns (beam current: 8 nA, beam diameter: 5 nm) for 15 s/point corresponding to a total dose of 4×10^{10} e/nm². (c) EELS spectra obtained from the irradiation point at the center of b (top panel) and the surroundings (bottom panel), which are compared to MLLS fitting curves composed of CsPbBr₃ and Cs₄PbBr₆ reference spectra. A tail of zero-loss peak was subtracted by fitting with a power law function. Measurement areas for the EELS spectra are indicated by squares in a. (d) CsPbBr₃ ratio map derived by MLLS fitting at each measurement point in an EELS mapping including the central nano-light source in b. The bottom panel shows a profile along the line indicated in the ratio map. The BF-STEM image and the CL map in a and b were obtained at a beam energy of 300 keV and a probe current of 200 pA, and the EELS mapping data for c and d were obtained at a beam energy of 80 keV and a probe current of 18 pA.

performed in the energy range of 1.4 to 6 eV, and in this energy range, no significant signals were expected from the Si₃N₄ or SiO₂ layers above and below the halide layer.^{37,38} The MLLS fitting indicates that the experimental spectrum at the irradiation point (EELS1) is well reproduced by summing the reference spectra of CsPbBr₃ and Cs₄PbBr₆, confirming the generation of a CsPbBr₃ particle, while the spectrum obtained far from the irradiation point (EELS2) is almost reproduced only using the reference spectrum of Cs₄PbBr₆. The generated CsPbBr₃ nanoparticle is visualized

as a CsPbBr_3 ratio map derived by the MLLS fitting at each measurement point, indicating the particle size of ~ 25 nm (Fig. 4d).

At the irradiation points, the sample thickness (or density) decreases as suggested by the bright spots observed in the BF-STEM image (Fig. 4a), and the generated CsPbBr_3 nanoparticles have different element ratios from the original Cs_4PbBr_6 phase. These facts raise the possibility of knock-on of specific elements by irradiating Cs_4PbBr_6 with an electron beam. Such local changes in the element ratios were confirmed by using EDS mapping under a low dose condition for a field

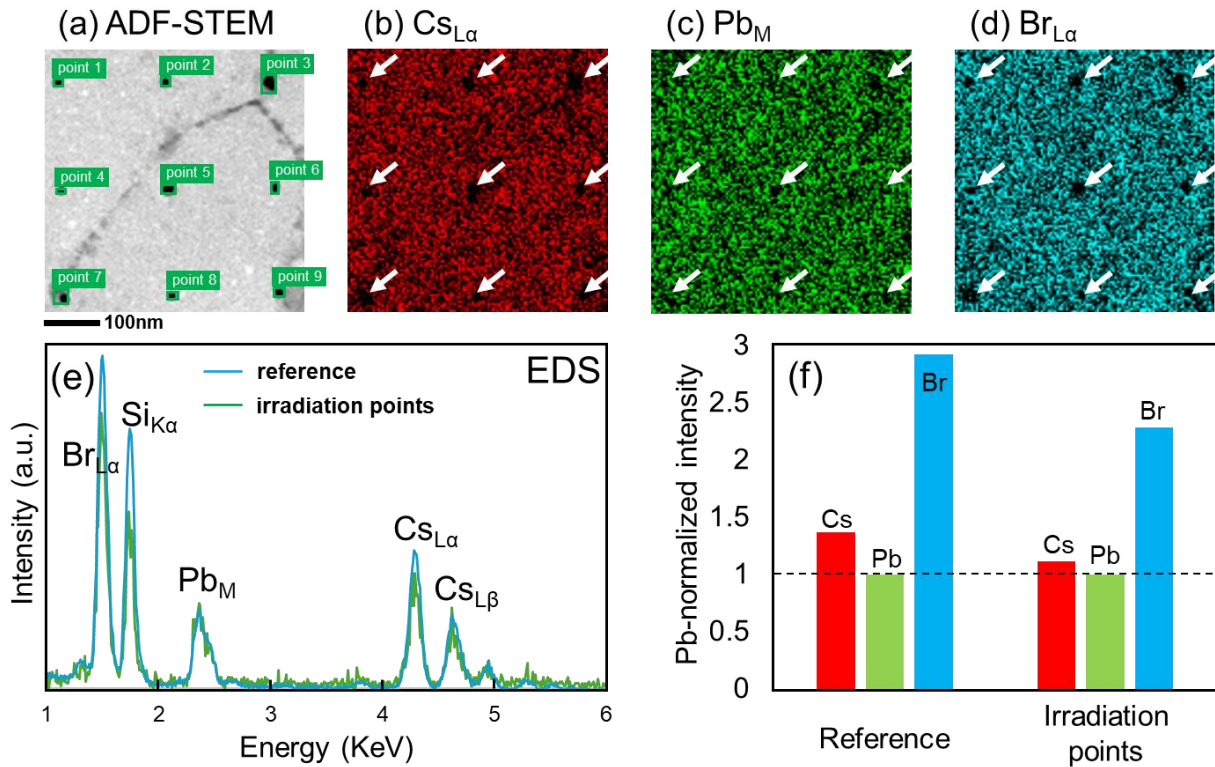


Figure 5 EDS analysis of the local element ratio change due to electron beam irradiation in the Cs_4PbBr_6 – CsBr film. (a) BF-STEM image obtained after point irradiation at a beam energy of 300 keV and a high dose rate of $6 \text{ e}/\text{nm}^2/\text{ns}$ (beam current: 3 nA, beam diameter: 1 nm) for 15 s/point corresponding to a total dose of $9 \times 10^{10} \text{ e}/\text{nm}^2$. (b–d) Elemental maps using X-ray intensities at Cs_{La} , Pb_M , and Br_{La} lines, respectively. The white arrows indicate the nine irradiation points. (e) EDS spectra averaged over nine extraction areas near the irradiation points (green curve) and extracted from reference Cs_4PbBr_6 grains far from this field of view (aqua curve). The nine extraction areas are indicated by rectangles in a. (f) Change in X-ray intensities between the two spectra in e, quantified by fitting Gaussian curves to Cs_{La} , Pb_M , and Br_{La} peaks. The intensities are normalized by Pb_M peak intensity. All the measurements here were performed at a beam energy of 300 keV and a probe current of 50 pA.

of view shown in Fig. 5a, where 9 points were irradiated under a high dose condition with a beam current of 3 nA and a beam diameter of 1 nm for 15 s/point in advance. Elemental maps using the X-ray intensities at the $\text{Cs}_{\text{L}\alpha}$, Pb_{M} , and $\text{Br}_{\text{L}\alpha}$ lines are shown in Figs. 5b–d, respectively. Due to the decrease in X-ray intensity, irradiation points (white arrows) are clearly recognized as dark spots in the Cs map (Fig. 5b) and Br map (Fig. 5d), while the intensity decrease is minor for Pb (Fig. 5c). This difference is clearer in a comparison of the EDS spectra; the $\text{Cs}_{\text{L}\alpha}$ and $\text{Br}_{\text{L}\alpha}$ peaks in the averaged spectrum extracted from the nine irradiation points are lower than those in the reference spectrum obtained from Cs_4PbBr_6 grains far from this field of view (Fig. 5e). Quantitative comparison normalized by Pb_{M} peak intensity reveals that the peak intensities of $\text{Cs}_{\text{L}\alpha}$ and $\text{Br}_{\text{L}\alpha}$ decrease by ~20% during the irradiation (Fig. 5f). This result indicates that electron beam irradiation preferentially knocks out Cs and Br atoms from Cs_4PbBr_6 , locally shifting the element ratios to $\text{Cs}:\text{Pb}:\text{Br} = 1:1:3$, stabilizing the CsPbBr_3 phase. Note that excessive irradiation can damage CsPbBr_3 nanoparticles as seen in a previous study.³⁹

Optimization of the irradiation time

To optimize the irradiation time and evaluate the performance of our proposed method, we obtained CL maps after irradiation for different irradiation times as shown in Figs. 6a–e. Irradiation points were selected on a 3×3 square lattice with a lattice spacing of ~210 nm, and each point was irradiated under a high dose condition with a beam current of 3 nA and a beam diameter of 4 nm for 5–25 seconds. Wavelength-filtered CL maps acquired at a low dose condition current are shown in Figs. 6a–e. When the irradiation time is 5 s/point, clear bright spots are observed at less than half of the points (Fig. 6a). At 10 s/point or more, bright spots were formed at all the points, and the spots become brighter overall with increasing the irradiation time (Figs. 6b–d). However,

some spots become significantly darker at 25 s/point (Fig. 6d) compared to 20 s/point, suggesting that the formed CsPbBr_3 nanoparticles are damaged by excessive irradiation.³⁹ To optimize the irradiation time, we evaluated the quality of each nano-light source generation as follows. The irradiation points were first estimated from BF-STEM images acquired after the irradiation. As mentioned above, the film thickness decreases due to the point irradiation, and the irradiation traces were observed as bright spots in the BF-STEM images (e.g. Fig. 4a). The positions of

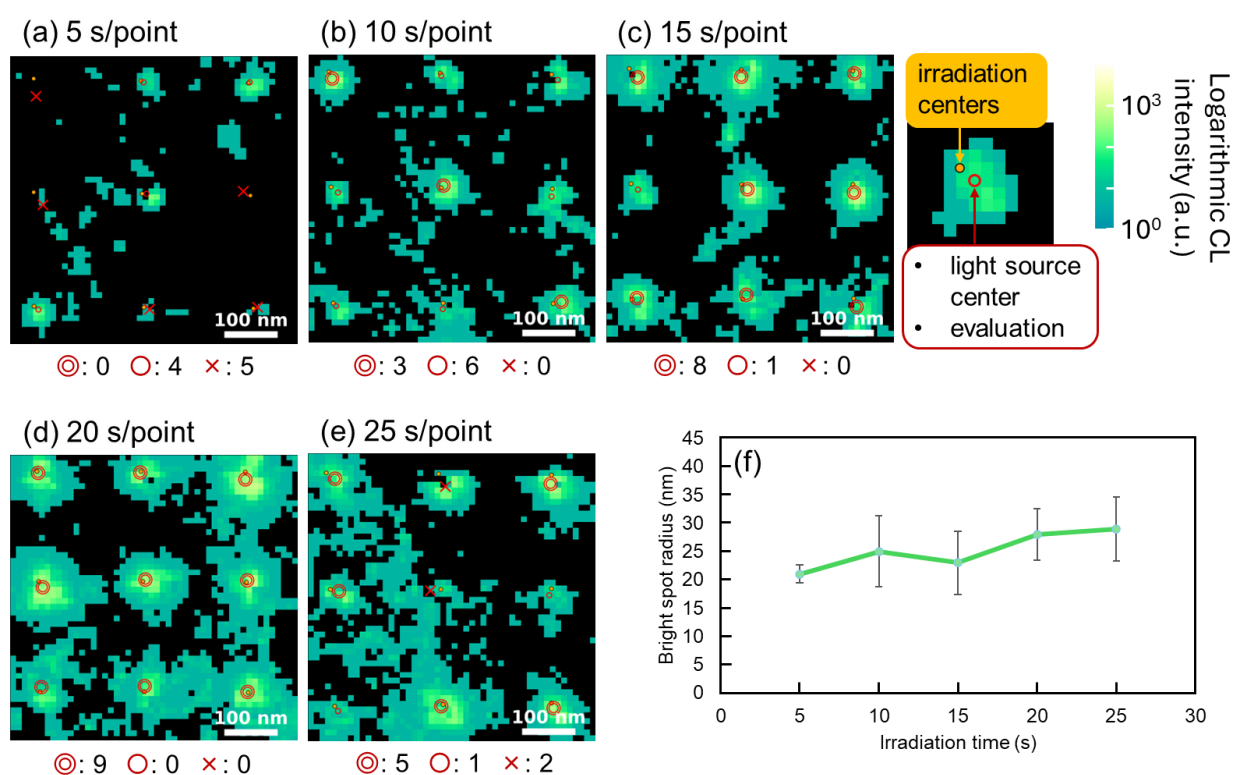


Figure 6 Optimization of the irradiation time. (a–e) CL maps (wavelength range: 500 to 550 nm) obtained from Cs_4PbBr_6 grains in the $\text{Cs}_4\text{PbBr}_6\text{--CsBr}$ film after point irradiation. Irradiation points were selected on a 3×3 square lattice with a lattice spacing of ~ 210 nm. Each point was irradiated with a beam energy of 300 keV, a beam current of 3 nA, and a beam diameter of 4 nm for 5–25 seconds. The inset on the right of c describes the marks near each irradiation point. The orange dots indicate the irradiation centers measured at the irradiation traces appearing in BF-STEM images obtained after the point irradiation. Quality of each point irradiation is classified into 3 levels "◎" (very successful), "○" (successful), and "✗" (failed) according to the criteria described in the main text, and these symbols are marked at each light source center \bar{r} in the CL maps. The number assigned to each level is displayed below each CL map. (f) Irradiation time dependence of average radius of generated nano-light sources. The failed points are excluded in this averaging. The error bars represent the standard deviation. All the measurements here were performed at a beam energy of 300 keV and a probe current of 200 pA.

irradiation centers are determined from the irradiation traces with an image process provided in Supporting Information. The brightness of each generated nano-light source is evaluated by the total CL intensity within the unit cell (square of ~ 210 nm side length) centered on the irradiation center. The center of nano-light source $\bar{\mathbf{r}}$ is defined as the weighted average $\bar{\mathbf{r}} = \sum I_{i,j} \mathbf{r}_{i,j} / \sum I_{i,j}$ using CL intensity $I_{i,j}$ and position $\mathbf{r}_{i,j}$ at each pixel within the unit cell. The radius of nano-light source Δr is defined as mean deviation $\Delta r = \sum I_{i,j} |\mathbf{r}_{i,j} - \bar{\mathbf{r}}| / \sum I_{i,j}$, which is calculated within the unit cell. We here evaluate the nano-light source generation as "successful" when the total CL intensity exceeds 10^2 , the light source center $\bar{\mathbf{r}}$ is located within 30 nm from the irradiation center, and the radius Δr is less than 40 nm or less. Among these, particularly bright sources with a total CL count exceeding 10^3 are evaluated as "very successful". These evaluations are indicated by marking a "○" and a "◎" at each center $\bar{\mathbf{r}}$ in the CL maps, respectively. When the above criteria are not met, an "×" is marked. According to the above evaluation criteria, an irradiation time of ~ 20 seconds corresponding to a total dose of $\sim 3 \times 10^{10}$ e/nm² is optimal.

The average radius of nano-light sources increases gradually with irradiation time, ranging from 20 nm to 30 nm (Fig. 6f). The standard deviation between the irradiation center and the light source center was evaluated to be 10 nm for irradiation time of 20 s/point. Therefore, the proposed method enables positioning light sources with a lateral size of several tens of nanometers and the lateral positional precision of 10 nm. The increase in source radius with irradiation time suggests that the source radius can be made smaller by controlling the irradiation in a shorter time range or a lower dose rate range. However, achieving such finer light source positioning requires development of an irradiation control system tailored to individual nucleation, including feedback of real-time CL measurements, since the time at which nucleation begins is highly fluctuated as suggested by the CL map at irradiation time of 5 s/point (Fig. 6a).

CONCLUSION

We fabricated the film mainly composed of Cs_4PbBr_6 excluding CsPbBr_3 , and demonstrated that a CsPbBr_3 nano-light source can be generated by irradiating Cs_4PbBr_6 with an electron beam. Our elemental analysis suggested that the electron beam preferentially knocked out Cs and Br atoms from Cs_4PbBr_6 , leading to the generation of CsPbBr_3 nanoparticles. Using this proposed method, we further demonstrated that nano-light sources with radii of several tens of nanometers can be arranged with the positional precision of 10 nm and submicron spacing. This method is based on evaporation and electron beam irradiation processes, and thus, is versatile enough to be integrated in various applications including on-chip optical devices.

METHODS

Fabrication of CsPbBr_3 – Cs_4PbBr_6 and Cs_4PbBr_6 – CsBr films

We first fabricated a CsPbBr_3 – Cs_4PbBr_6 nanocomposite film on a Si_3N_4 (20 nm thick) film substrate (SiMPore, USA) in a similar manner as previous studies.^{23,28} After depositing SiO_2 layer (5 nm thick) on the Si_3N_4 film substrate by radio frequency (RF) magnetron sputtering to obtain a clean surface, CsPbBr_3 – Cs_4PbBr_6 nanocomposite layer (140 nm thick) was deposited by thermal evaporation. The evaporation source for the CsPbBr_3 – Cs_4PbBr_6 deposition was synthesized based on the protocol proposed previously.²⁵ PbBr_2 (0.22 mmol, $\geq 98\%$, Sigma-Aldrich) and cesium acetate (0.88 mmol, 99.9% trace metals basis, Sigma-Aldrich) were stirred in dimethyl sulfoxide (0.5 ml, anhydrous, $\geq 99.9\%$, Sigma-Aldrich) for 1 h. After adding 0.1 mL aqueous HBr solution (48% by weight in H_2O , Sigma-Aldrich), the mixed solution was stirred for 12 h. The precipitation was separated from the mixed solution by centrifugation, and the powder was dried under vacuum

overnight. To prevent degradation due to air exposure, the top surface of the CsPbBr_3 – Cs_4PbBr_6 nanocomposite layer was covered with a 10 nm thick SiO_2 layer by RF magnetron sputtering. Overall, a SiO_2 (10 nm)/ CsPbBr_3 – Cs_4PbBr_6 (140 nm)/ SiO_2 (5 nm)/ Si_3N_4 (20 nm) multilayer film was fabricated. All the above procedures were done at room temperature. Then, this multilayer film was annealed in vacuum at 250 °C for 30 min to obtain a structure separated into CsPbBr_3 and Cs_4PbBr_6 grains with sizes from several hundred nanometers to micrometers as shown in Figs. 1a and b.

The Cs_4PbBr_6 – CsBr film used in this study was fabricated with the same process as above, except that the element ratios were tuned by adding 23 wt% CsBr powder to the CsPbBr_3 – Cs_4PbBr_6 evaporation source. Overall, a SiO_2 (10 nm)/ Cs_4PbBr_6 – CsBr (160 nm)/ SiO_2 (5 nm)/ Si_3N_4 (20 nm) multilayer film was fabricated. This multilayer film was also annealed in vacuum at 250 °C for 30 min.

STEM-based spectroscopy and point irradiation with a focused electron beam

CL analysis was performed at a beam energy of 300 keV, a beam current of 200 pA, and a beam diameter of 2 nm using a modified transmission electron microscope JEM-3200FSK (JEOL). The details of the CL optics are provided in a previous study.²⁸ A CL mapping system was newly implemented in this study, which is based on a single photon counting detector linked to the beam scan. The exposure time per pixel was 50 ms. A bandpass filter with a wavelength range of 500 to 550 nm was used to highlight CsPbBr_3 nanoparticles or grains.

EELS and EDS analyses were performed at beam energies of 80 or 300 keV, a beam current of 18 or 50 pA, and a sub-nanometer beam diameter using a transmission electron microscope Titan Cubed G2 60-300 (Thermo Fisher Scientific, USA) equipped with an aberration

corrector for the probe forming lens system, a monochromator and an energy filter Quantum 965 (Gatan, USA) for EELS, and four-quadrant windowless super-X silicon drift detectors for EDS. By using the monochromator, the energy resolution was improved to 0.14 eV measured from the full width at half maximum of zero-loss peak (ZLP). The exposure time per pixel for EELS mapping was 50 ms. The typical dwell time for EDS mapping was on the order of 10 microseconds.

Point irradiation was mainly performed with a beam energy of 300 keV, beam currents of 3 or 8 nA, and beam diameters of 4 or 5 nm using JEM-3200FSK. Only for EDS analysis (Fig. 5), point irradiation was performed with a beam energy of 300 keV, a beam current of 3 nA, and a beam diameter of 1 nm using Titan Cubed G2 60-300.

All the experiments using electron microscopes were performed at room temperature.

CONFLICT OF INTEREST

The authors declare no competing financial interest.

ACKNOWLEDGMENTS

We would like to thank Keiichirou Akiba and Takumi Sannomiya for valuable discussion on this study. Annealing of the samples was supported by Shiro Ihara and Mitsuhiro Murayama. This study was supported by JSPS KAKENHI Grant Numbers JP25K01640, JP23K17350, JP23K23196, JP22H05034. We would also like to mention that preliminary experiments of this study were conducted at the Institute for Chemical Research, Kyoto University, supported by “Advanced Research Infrastructure for Materials and Nanotechnology in Japan (ARIM)” of the Ministry of Education, Culture, Sports, Science and Technology (MEXT) and International Collaborative Research Program of Institute for Chemical Research, Kyoto University (grant #

2025-141).

REFERENCES

1. Santhosh, K.; Bitton, O.; Chuntonov, L.; Haran, G. Vacuum Rabi Splitting in a Plasmonic Cavity at the Single Quantum Emitter Limit. *Nat. Commun.* **2016**, *7*, 11823.
2. Imada, H.; Miwa, K.; Imai-Imada, M.; Kawahara, S.; Kimura, K.; Kim, Y. Single-Molecule Investigation of Energy Dynamics in a Coupled Plasmon-Exciton System. *Phys. Rev. Lett.* **2017**, *119*, 013901.
3. Leng, H.; Szychowski, B.; Daniel, M.-C.; Pelton, M. Strong Coupling and Induced Transparency at Room Temperature with Single Quantum Dots and Gap Plasmons. *Nat. Commun.* **2018**, *9*, 4012.
4. Söllner, I.; Mahmoodian, S.; Hansen, S. L.; Midolo, L.; Javadi, A.; Kiršanskė, G.; Pregnolato, T.; El-Ella, H.; Lee, E. H.; Song, J. D.; Stobbe, S.; Lodahl, P. Deterministic Photon–Emitter Coupling in Chiral Photonic Circuits. *Nat. Nanotechnol.* **2015**, *10*, 775–778.
5. Barik, S.; Karasahin, A.; Flower, C.; Cai, T.; Miyake, H.; DeGottardi, W.; Hafezi, M.; Waks, E. A Topological Quantum Optics Interface. *Science* **2018**, *359*, 666–668.
6. Mehrabad, M. J.; Foster, A. P.; Dost, R.; Clarke, E.; Patil, P. K.; Fox, A. M.; Skolnick, M.; Wilson, L. R. Chiral Topological Photonics with an Embedded Quantum Emitter. *Optica* **2020**, *7*, 1690–1696.
7. Esmaeil Zadeh, I.; Elshaari, A. W.; Jöns, K. D.; Fognini, A.; Dalacu, D.; Poole, P. J.; Reimer, M. E.; Zwiller, V. Deterministic Integration of Single Photon Sources in Silicon Based Photonic Circuits. *Nano Lett.* **2016**, *16*, 2289–2294.

8. Davanco, M.; Liu, J.; Sapienza, L.; Zhang, C.-Z.; De Miranda Cardoso, J. V.; Verma, V.; Mirin, R.; Nam, S. W.; Liu, L.; Srinivasan, K. Heterogeneous Integration for On-Chip Quantum Photonic Circuits with Single Quantum Dot Devices. *Nat. Commun.* **2017**, *8*, 889.
9. Schnauber, P.; Schall, J.; Bounouar, S.; Höhne, T.; Park, S.-I.; Ryu, G.-H.; Heindel, T.; Burger, S.; Song, J.-D.; Rodt, S.; Reitzenstein, S. Deterministic Integration of Quantum Dots into on-Chip Multimode Interference Beamsplitters Using in Situ Electron Beam Lithography. *Nano Lett.* **2018**, *18*, 2336–2342.
10. Li, S.; Yang, Y.; Schall, J.; von Helversen, M.; Palekar, C.; Liu, H.; Roche, L.; Rodt, S.; Ni, H.; Zhang, Y.; Niu, Z.; Reitzenstein, S. Scalable Deterministic Integration of Two Quantum Dots into an On-Chip Quantum Circuit. *ACS Photonics* **2023**, *10*, 2846–2853.
11. Luo, Y.; Shepard, G. D.; Ardelean, J. V.; Rhodes, D. A.; Kim, B.; Barmak, K.; Hone, J. C.; Strauf, S. Deterministic Coupling of Site-Controlled Quantum Emitters in Monolayer WSe₂ to Plasmonic Nanocavities. *Nat. Nanotechnol.* **2018**, *13*, 1137–1142.
12. Lee, S.-J.; So, J.-P.; Kim, R. M.; Kim, K.-H.; Rha, H.-H.; Na, G.; Han, J. H.; Jeong, K.-Y.; Nam, K. T.; Park, H.-G. Spin Angular Momentum–Encoded Single-Photon Emitters in a Chiral Nanoparticle-Coupled WSe₂ Monolayer. *Sci. Adv.* **2024**, *10*, eadn7210.
13. Luo, M.; Ge, J.; Huang, P.; Yu, Y.; Seo, I. C.; Lu, K.; Sun, H.; Tan, J. K.; Tay, B. K.; Kim, S.; Gao, W.; Li, H.; Nam, D. Deterministic Formation of Carbon-Functionalized Quantum Emitters in Hexagonal Boron Nitride. *Nat. Commun.* **2025**, *16*, 11450.
14. Glushkov, E.; Macha, M.; Räth, E.; Navikas, V.; Ronceray, N.; Cheon, C. Y.; Ahmed, A.; Avsar, A.; Watanabe, K.; Taniguchi, T.; Shorubalko, I.; Kis, A.; Fantner, G.; Radenovic, A. Engineering Optically Active Defects in Hexagonal Boron Nitride Using Focused Ion Beam and Water. *ACS Nano* **2022**, *16*, 3695–3703.

15. Gale, A.; Li, C.; Chen, Y.; Watanabe, K.; Taniguchi, T.; Aharonovich, I.; Toth, M. Site-Specific Fabrication of Blue Quantum Emitters in Hexagonal Boron Nitride. *ACS Photonics* **2022**, *9*, 2170–2177.

16. Gan, L.; Zhang, D.; Zhang, R.; Zhang, Q.; Sun, H.; Li, Y.; Ning, C.-Z. Large-Scale, High-Yield Laser Fabrication of Bright and Pure Single-Photon Emitters at Room Temperature in Hexagonal Boron Nitride. *ACS Nano* **2022**, *16*, 14254–14261.

17. Lin, K.; Xing, J.; Quan, L. N.; García de Arquer, F. P.; Gong, X.; Lu, J.; Xie, L.; Zhao, W.; Zhang, D.; Yan, C.; Li, W.; Liu, X.; Lu, Y.; Kirman, J.; Sargent, E. H.; Xiong, Q.; Wei, Z. Perovskite light-emitting diodes with external quantum efficiency exceeding 20 per cent. *Nature* **2018**, *562*, 245–248.

18. Lian, Y.; Wang, Y.; Yuan, Y.; Ren, Z.; Tang, W.; Liu, Z.; Xing, S.; Ji, K.; Yuan, B.; Yang, Y.; Gao, Y.; Zhang, S.; Zhou, K.; Zhang, G.; Stranks, S. D.; Zhao, B.; Di, D. Downscaling micro- and nano-perovskite LEDs. *Nature* **2025**, *640*, 62–68.

19. Schlaus, A. P.; Spencer, M. S.; Miyata, K.; Liu, F.; Wang, X.; Datta, I.; Lipson, M.; Pan, A.; Zhu, X.-Y. How lasing happens in CsPbBr_3 perovskite nanowires. *Nat. Commun.* **2019**, *10*, 265.

20. Tiguntseva, E.; Koshelev, K.; Furasova, A.; Tonkaev, P.; Mikhailovskii, V.; Ushakova, E. V.; Baranov, D. G.; Shegai, T.; Zakhidov, A. A.; Kivshar, Y.; Makarov, S. V. Room-Temperature Lasing from Mie-Resonant Nonplasmonic Nanoparticles. *ACS Nano* **2020**, *14*, 8149–8156.

21. Park, Y.-S.; Guo, S.; Makarov, N. S.; Klimov, V. I. Room-Temperature Single-Photon Emission from Individual Perovskite Quantum Dots. *ACS Nano* **2015**, *9*, 10386–10393.

22. Murali, R.; Panda, M. K.; Challa, R. K.; Acharjee, D.; Rao Soma, V.; Ghosh, S.; Raavi, S. S. K. Bright and Stable Single-Photon Emission in Zinc-Alloyed CsPbBr_3 Nanocrystals Through Controlled Auger Recombination. *Small* **2025**, 22, e05011.

23. Saito, H.; Kihara, K.; Ikeuchi, M.; Yanagimoto, S.; Kubota, T.; Akiba, K.; Sannomiya, T. Nano-light source generation by electron beam irradiation of $\text{CsPbBr}_3/\text{Cs}_4\text{PbBr}_6$ composites. *Appl. Phys. Lett.* **2025**, 127, 261102.

24. Kang, B.; Biswas, K. Exploring Polaronic, Excitonic Structures and Luminescence in $\text{Cs}_4\text{PbBr}_6/\text{CsPbBr}_3$. *J. Phys. Chem. Lett.* **2018**, 9, 830–836.

25. Chen, Y.-M.; Zhou, Y.; Zhao, Q.; Zhang, J.-Y.; Ma, J.-P.; Xuan, T.-T.; Guo, S.-Q.; Yong, Z.-J.; Wang, J.; Kuroiwa, Y.; Moriyoshi, C.; Sun, H.-T. *$\text{Cs}_4\text{PbBr}_6/\text{CsPbBr}_3$ Perovskite Composites with Near-Unity Luminescence Quantum Yield: Large-Scale Synthesis, Luminescence and Formation Mechanism, and White Light-Emitting Diode Application*. *ACS Appl. Mater. Interfaces* **2018**, 10, 15905–15912.

26. Xu, J.; Huang, W.; Li, P.; Onken, D. R.; Dun, C.; Guo, Y.; Ucer, K. B.; Lu, C.; Wang, H.; Geyer, S. M.; Williams, R. T.; Carroll, D. L. Imbedded Nanocrystals of CsPbBr_3 in Cs_4PbBr_6 : Kinetics, Enhanced Oscillator Strength, and Application in Light-Emitting Diodes. *Adv. Mater.* **2017**, 29, 1703703.

27. Zheng, S.; Wang, Z.; Jiang, N.; Huang, H.; Wu, X.; Li, D.; Teng, Q.; Li, J.; Li, C.; Li, J.; Pang, T.; Zeng, L.; Zhang, R.; Huang, F.; Lei, L.; Wu, T.; Yuan, F.; Chen, D. Ultralow voltage–driven efficient and stable perovskite light-emitting diodes. *Sci. Adv.* **2024**, 10, eadp8473.

28. Fujimaru, T.; Tanaka, H.; Inamata, M.; Ikeuchi, M.; Yamashita, H.; Miyazaki, H.; Gondo, T.; Hata, S.; Murayama, M.; Saito, H. Light Emission Enhancement on Nanostructured

Surfaces Quantitatively Evaluated by Cathodoluminescence Coincidence Counting. *ACS Photonics* **2025**, 12, 3073–3081.

29. Nekita, S.; Yanagimoto, S.; Sannomiya, T.; Akiba, K.; Takiguchi, M.; Sumikura, H.; Takagi, I.; Nakamura, K. G.; Yip, S. P.; Meng, Y.; Ho, J. C.; Okuyama, T.; Murayama, M.; Saito, H. Diffusion-Dominated Luminescence Dynamics of CsPbBr_3 Studied Using Cathodoluminescence and Microphotoluminescence Spectroscopy. *Nano Lett.* **2024**, 24, 3971–3977.

30. Riesen, N.; Lockrey, M.; Badek, K.; Riesen, H. On the origins of the green luminescence in the “zero-dimensional perovskite” Cs_4PbBr_6 : conclusive results from cathodoluminescence imaging. *Nanoscale* **2019**, 11, 3925.

31. de Weerd, C.; Lin, J.; Gomez, L.; Fujiwara, Y.; Suenaga, K.; Gregorkiewicz, T. Hybridization of Single Nanocrystals of Cs_4PbBr_6 and CsPbBr_3 . *J. Phys. Chem. C* **2017**, 121, 19490–19496.

32. Kiguchi, M.; Entani, S.; Saiki, K.; Koma, A. Atomic and electronic structure of CsBr film grown on LiF and KBr . *Surf. Sci.* **2003**, 523, 73–79.

33. Xu, F.; Kong, X.; Wang, W.; Juan, F.; Wang, M.; Wei, H.; Li, J.; Cao, B. Quantum size effect and surface defect passivation in size-controlled CsPbBr_3 quantum dots. *J. Alloys Compd.* **2020**, 831, 154834.

34. Chen, J.; Žídek, K.; Chábera, P.; Liu, D.; Cheng, P.; Nuutila, L.; Al-Marri, M. J.; Lehtivuori, H.; Messing, M. E.; Han, K.; Zheng, K.; Pullerits, T. Size- and wavelength-dependent two-photon absorption cross-section of CsPbBr_3 perovskite quantum dots. *J. Phys. Chem. Lett.* **2017**, 8, 2316–2321.

35. Kubota, T.; Yanagimoto, S.; Saito, H.; Akiba, K.; Ishii, A.; Sannomiya, T. Cathodoluminescence spectral and lifetime mapping of Cs_4PbBr_6 : fast lifetime and its scintillator application. *Appl. Phys. Express* **2024**, 17, 015005.

36. Cao, F.; Yu, D.; Ma, W.; Xu, X.; Cai, B.; Yang, Y. M.; Liu, S.; He, L.; Ke, Y.; Lan, S.; Choy, K.-L.; Zeng, H. Shining Emitter in a Stable Host: Design of Halide Perovskite Scintillators for X-ray Imaging from Commercial Concept. *ACS Nano* **2020**, 14, 5183–5193.

37. Asano, T.; Tezura, M.; Saitoh, M.; Tanaka, H.; Kikkawa, J.; Kimoto, K. Nanoscale observation of subgap excitations in $\beta\text{-Si}_3\text{N}_4$ with a high refractive index using low-voltage monochromated STEM: a new approach to analyze the physical properties of defects in dielectric materials. *Appl. Phys. Express* **2022**, 15, 076501.

38. Park, J.; Heo, S.; Chung, J.-G.; Kim, H.; Lee, H.; Kim, K.; Park, G.-S. Bandgap measurement of thin dielectric films using monochromated STEM-EELS. *Ultramicroscopy* **2009**, 109, 1183–1188.

39. Dang, Z.; Shamsi, J.; Palazon, F.; Imran, M.; Akkerman, Q. A.; Park, S.; Bertoni, G.; Prato, M.; Brescia, R.; Manna, L. In Situ Transmission Electron Microscopy Study of Electron Beam-Induced Transformations in Colloidal Cesium Lead Halide Perovskite Nanocrystals. *ACS Nano* **2017**, 11, 2124–2132.

SUPPORTING INFORMATION

A. Positions of irradiation centers

The positions of irradiation centers shown in Figs. 6a–e of the main text were estimated from irradiation traces observed in BF-STEM images. The procedure is explained below using an example of the irradiation time of 20 s/points. Figure S1a shows a BF-STEM image acquired after the point irradiation, in which nine irradiation traces are arranged in the form of a 3×3 square lattice. These illumination traces were clearly separated from the background by binarization (Fig. S1b). The positions of irradiation centers at the four corners (circled in yellow) were estimated from the average position calculated within each bright spot, and their midpoints were assumed to be the positions of the other five irradiation centers.

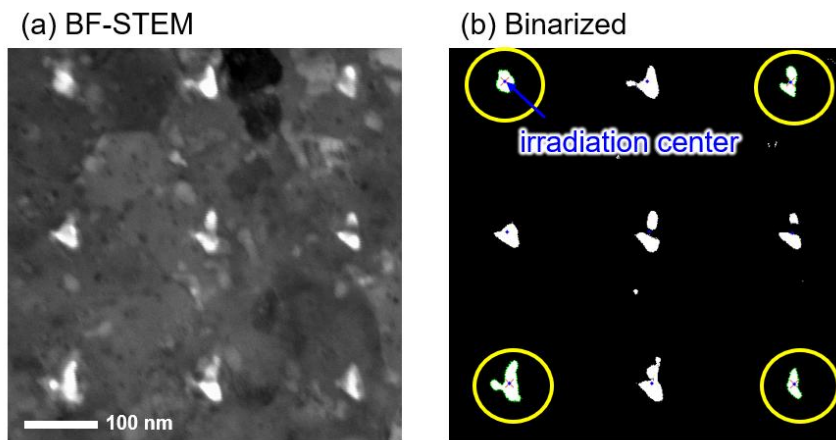


Figure S1 (a) BF-STEM image acquired after point irradiation for an irradiation time of 20 s/points. (b) Binarized image of the BF-STEM image in (a). The estimated positions of irradiation centers are indicated by blue dots.